Virtual Anodes in Ion Beam Emissions in Space: Numerical Simulations

Joseph Wang

Jet Propulsion Laboratory

California Institute of Technology, Pasadena, CA 91109

Shu T. Lai

Phillips Laboratory, Hanscom AFB, MA 01731

1. Introduction

Many space experiments and applications involve plasma beam emissions. For instance, electron and ion beam experiments have been conducted to study study beam-plasma interactions, neutralization processes, spacecraft charging and discharge, etc This paper is concerned with the physics of ion beam emissions from spacecraft to a low density space plasma. The emphasis is on space charge effects.

Most ion beam devices tc)-date are similar to ion thrusters (see Figure I). In an ion thruster, the ions are accelerated electrostatically by a biased grid to form a high velocity beam, typically in the keV energy range. When an ion thruster is used for propulsion purpose, the ion beam is neutralized by electrons emitted from the neutralizer. Hence, the beam flow is quasi neutral. When an ion thruster is used for ion beam experiments, the neutralizer is turned off. If beam current density far exceeds that of the space plasma, the beam flow becomes a space charge flow.

The properties of a space charge flow was first studied for high current density beams between two plane electrodes (i.e. diodes, first studied by *Child*[1911]). It is instructive 10 review the classical diode theory. 111 a diode, a charged particle beam is emitted from an electrode towards another electrode in a vacuum tube. The physics of beam flow in a diode was presented in the classical theories of *Salzberg and Haeff*[1938] and *Fay et al.*[1938]. Consider an ion beam flow from a cathode towards an anode. At low current density, the potential profile along the charge flow is monotonic. When the current density increases, so is the importance of the space charge. For the special case of zero initial flow velocity, the current density is limited by Child's law, In this case, the space charge prohibits further increase in current density, and the potential profile is always monotonic. For nonzero initial velocity in space charge flows, the potential profile can become non-monotonic with a potential hump appears in between the two electrodes. At sufficiently large current density, the potential hump may become so high that the kinetic energy of the flowing charge is zero at the hump When this happens, some charges go backwards and some forwards. As a result, only part of the emitting current can be transmitted while the rest is reflected backwards. Therefore, this potential hump behaves as a virtual electrode. This behavior has been confirmed in diode tubes.

Lai et al.[1979, 1989] suggested that this behavior may also occur in beam emissions in space. For ion beam emissions in space, since the spacecraft is charged negatively with respect 10 the ambient, the spacecraft serves as a cathode and the ambient serves as an anode. *Lai et al.*[1979] studied the currc]]t-voltage characteristics during positive ion beam emissions 011 the SCATHA satellite. They found at low currents, the amplitude of the (negative) spacecraft potential increased. The potential amplitude peaked at an intermediate current. When the current is increased further, the potential dropped to a low value. Hence, it was postulated that a virtual anode may have formed in front of the beam device blocking partly the beam transmission. Some features of virtual anode in ion beams have also been discussed by *Stannard et al.*[1981].

However, ion beam emission in space is far more complex than the classical diode problem. For instance, in diodes, the electrodes are at fixed locations and potentials, and the beam flow is essentially a 1-dimension problem. While for ion beam emission in space, both the spacecraft potential and the location where the po-

tential inside the beam approaches the ambient potential are variables, and the problem is inherently a 3-dimensional one where beam divergence due to space charge effect and the potential sheath profile play an important role. It is obvious that the resulting interaction cannot be treated adequately by the classical theory of space charge flow.

In this paper we apply three-dimensional particle simulations to study the problem of ion beam emissions in space and examine the virtual anode concept for 3-D space charge flow. A 1-D analytical theory of space charge flow is first presented in Section 2. 3-D particle simulation results are discussed in Section 3. Section 4 contains a summary and conclusions.

2. 1-D Theory of Space Charge Flow

We first discuss the one-dimensional theory of space charge flow of an ion beam. Consider the situation illustrated in Fig. 2a: an ion beam is emitted from a plane electrode at $x = 0$ and received by a plane electrode at $x = L$. The initial beam particle kinetic energy is $e\Phi_{b0} = \frac{1}{2}mv_0^2$, and the emitting current density $J_0 = en_0v_0$. We take the potential at the two ends to be $\Phi(x = 0) = \Phi_s$, and $\Phi(x = L) = 0$. The solution to this problem follows the classical theory first presented by *Fay et al.*[1938].

The governing equations are the Poisson's equation, current continuity, and energy conservation equation:

$$\frac{d^2\Phi}{dx^2} = -\frac{en}{\epsilon_0} \tag{1}$$

$$n = \frac{J_0}{ev} \tag{2}$$

$$e\Phi_{b0} = \frac{1}{2}mv_0^2 + e\Phi_s = \frac{1}{2}mv^2 + e\Phi \tag{3}$$

where $e\Phi_{b0}$ is the total beam particle energy. The particle velocity is given by

$$v = \sqrt{\frac{2e}{m}(\Phi_{b0} - \Phi)}$$

Hence, the ion beam is transmitted only when $\Phi_{b0} - \Phi > 0$. The differential equation for the space charge flow problem is

$$\frac{d^2\Phi}{dx^2} = -\frac{J_0}{\epsilon_0}\frac{1}{\sqrt{\frac{2e}{m}(\Phi_{b0} - \Phi)}} \tag{4}$$

Eq(4) is readily integrated to

$$\left(\frac{d\Phi}{dx}\right)^2\Big|_1^2 = -\frac{2J_0}{\epsilon_0}\sqrt{\frac{2m}{e}}\sqrt{\Phi_{b0} - \Phi}\Big|_{\Phi 1}^{\Phi 2} \tag{5}$$

One family of the solutions to eq(5) is for a monotonic potential profile $\Phi(x)$. For instance, consider the case $\Phi_s > 0$ and $v_0 = 0$ (i.e. $\Phi_{b0} = \Phi_s$ and $d\Phi/dx = 0$ at $x = 0$). Then from eq(5) we have

$$\frac{d\Phi}{dx} = -\sqrt{\frac{2J_0}{\epsilon_0}}\sqrt{\frac{2m}{e}}(\Phi_{b0} - \Phi)^{1/4} \tag{6}$$

which leads to

$$J_0 = \frac{4}{9}\sqrt{\frac{2e}{m}}\frac{\epsilon_0\Phi_s^{3/2}}{L^2} \tag{7}$$

This is the well-kllowll Child-Langmuir law of space charge limited current in a plane diode.

A more general solutions to eq(5) is for a nonmonotonic potential profile, where the potential takes a maximum at $x = x_m$, $\Phi(x_m) = \Phi_m > 0$. Let us define the following dimensionless variables: $\hat{x} = x/L$, $\hat{\Phi} = \Phi/\Phi_{b0}$, and $\hat{J}_0 = J_0/J_c$, where

$$J_c = \frac{4}{9}\sqrt{\frac{2e}{m}}\frac{\epsilon_0\Phi_{b0}^{3/2}}{L^2} \tag{8}$$

is the space charge limit current for a potential Φ_{b0}. Then, eq(4) is rewritten as

$$\frac{d^2\hat{\Phi}}{d\hat{x}^2} = -\frac{4}{9}\frac{\hat{J}_0}{(1 - \hat{\Phi})}$$

Integrating between $\hat{x}$ and $\hat{x}_m$ $(d\Phi/dx(x_m) = 0)$ leads to

$$\left(\frac{d\hat{\Phi}}{d\hat{x}}\right)^2 = \left(\frac{4}{3}\right)^2\hat{J}_0(\sqrt{1 - \hat{\Phi}} - \sqrt{1 - \hat{\Phi}_m}) \tag{9}$$

Since $d\Phi/dx$ has a different sign on each side of x_m, we have

$$\frac{d\hat{\Phi}}{d\hat{x}} = \frac{4}{3}\sqrt{\hat{J}_0}(\sqrt{1 - \hat{\Phi}} - \sqrt{1 - \hat{\Phi}_m})^{1/2}, \quad 0 < \hat{x} < \hat{x}_m \tag{10}$$

$$\frac{d\hat{\Phi}}{d\hat{x}} = -\frac{4}{3}\sqrt{\hat{J}_0}(\sqrt{1 - \hat{\Phi}} - \sqrt{1 - \hat{\Phi}_m})^{1/2}, \quad \hat{x}_m < \hat{x} < 1 \tag{11}$$

Integrating

$$\frac{d\hat{\Phi}}{(\sqrt{\hat{\Phi}_{b0} - \hat{\Phi}} - \sqrt{\Phi_{b0} - \hat{\Phi}_m})^{1/2}} = \pm\frac{4}{3}\sqrt{\hat{J}_0}d\hat{x}$$

in $[0, x_1]$ and $[\hat{x}_m, 1]$ respectively, one obtains

$$\sqrt{\hat{J}_0}\hat{x}_m = (\sqrt{\Phi_{bk0}} + 2\sqrt{1 - \hat{\Phi}_m})\sqrt{\sqrt{\Phi_{bk0}} - \sqrt{1 - \hat{\Phi}_m}} \tag{12}$$

$$\sqrt{\hat{J}_0}(1 - \hat{x}_m) = (1 + 2\sqrt{1 - \hat{\Phi}_m})\sqrt{1 - \sqrt{1 - \hat{\Phi}_m}} \tag{13}$$

where $\hat{\Phi}_{bk0} = mv_0^2/(2e\Phi_{b0}) = 1 - \hat{\Phi}_s$. Therefore,

$$\frac{1-\hat{x}_m}{x_m} = \frac{(1+2\sqrt{1-\hat{\Phi}_m})\sqrt{1-\sqrt{1-\hat{\Phi}_m}}}{(\sqrt{\hat{\Phi}_{bk0}}+2\sqrt{1-\hat{\Phi}_m})\sqrt{\sqrt{\hat{\Phi}_{bk0}}-\sqrt{1-\hat{\Phi}_m}}} \quad (14)$$

From eq(14), one finds

$$0 \le \hat{x}_m \le 0.5, \quad \hat{\Phi}_s \ge 0$$

$$0.5 \le \hat{x}_m \le 1, \quad \hat{\Phi}_s \le 0$$

$\hat{x}_m = 0.5$ for the special case $\hat{\Phi}_s = 0$.

In the limiting case $1 - \hat{\Phi}_m = 0$ (i.e. $\Phi_m = \frac{m}{2e}v_0^2 + \Phi_s$), the ion beam comes to a halt at x_m, $v(x_m) = 0$. In this case, some ions may be reflected back at x_m, while others are accelerated away in the x direction. Let f be the fraction of J_0 that is transmitted through this potential barrier. Then, the beam number density is

$$n = \frac{J_0}{ev} + \frac{(1-f)J_0}{ev}, \quad 0 < \hat{x} < \hat{x}_m$$

$$n = \frac{fJ_0}{ev}, \quad \hat{x}_m < \hat{x} < 1$$

Hence eq(10) and eq(11) become

$$\frac{d\hat{\Phi}}{(1-\hat{\Phi})^{1/4}} = \frac{4}{3}(2-f)\hat{J}_0 d\hat{x} \quad (15)$$

$$\frac{d\hat{\Phi}}{(1-\hat{\Phi})^{1/4}} = \frac{4}{3}f\hat{J}_0 d\hat{x} \quad (16)$$

They lead to

$$\sqrt{(2-f)\hat{J}_0}\hat{x}_m = \hat{\Phi}_{bk0}^{3/4}, \quad \sqrt{f\hat{J}_0}(1-\hat{x}_m) = 1 \quad (17)$$

or, in the dimensional form,

$$(2-f)J_0 = \frac{4}{9}\sqrt{\frac{2e}{m}}\frac{\epsilon_0(\Phi_{b0}-\Phi_s)^{3/2}}{x_m^2} = \frac{2}{9}\frac{m\epsilon_0}{e}\frac{v_0^{3/2}}{x_m^2} \quad (18)$$

$$fJ_0 = \frac{4}{9}\sqrt{\frac{2e}{m}}\frac{\epsilon_0\Phi_{b0}^{3/2}}{(L-x_m)^2} = \frac{2}{9}\frac{m\epsilon_0}{e}\frac{v_0^{3/2}(1+\frac{2e\Phi_s}{mv_0^2})^{3/2}}{(L-x_m)^2} \quad (19)$$

Note f is determined self-consistently by the space-charge current limit stated in the above two equations. The maximum current that can be transmitted to $x = L$ is $fJ_0 = J_c$ regardless of the emitting current. Therefore, when the emitting current $J_0 > J_c$, the potential hump Φ_m serves as a virtual anode. Hence, J_c represents a critical current density.

Now we consider an ion beam emitted into a low density ambient plasma, as illustrated in Fig. 2b. For this situation, the right side boundary condition becomes

$$\Phi(\infty) = 0, \quad \frac{d\Phi}{dx}(\infty) = 0$$

If there were a positive potential hump, the electrons would move in to neutralize the excess ion space charge. However, since the electron current J_e is limited by the ambient conditions, a nonmonotonic potential profile can still exist for strong ion beam emissions. Let us the divide the domain into a region I, $x < x_{inf}$, and a region II, $x_{inf} < x < \infty$. x_{inf} is the inflection point where the net charge is zero. There is a net ion charge surplus in region I ($d^2\Phi/dx^2 < 0$) and a net electron charge surplus in region II ($d^2\Phi/dx^2 < 0$).

If one knew x_{inf} *a priori*, the analysis for an ion beam between two plane electrodes can be applied in region I. The critical current density J_c is given by

$$J_c = \frac{4}{9}\sqrt{\frac{2e}{m}}\frac{\epsilon_0\Phi_{b0}^{3/2}}{x_{inf}^2}$$

However, in order to determine x_{inf}, one needs to resolve the detailed interactions between the ion beam and the ambient plasma. In addition, the beam divergence due to space charge effect may make the 1-D assumption unacceptable. Therefore, we shall attack the problem through particle simulations.

3. 3-D Particle Simulations

We have developed a set of Particle-in-cell (PIC) and Particle-in-cell with Monte Carlo collision (PIC-MCC) codes for ion thruster plasma interactions [*Wang and Brophy*, 1995c; *Wang et al*, 1996b], active space plasma experiments [*Wang et al*, 1996a], and other larger scale plasma simulations [*Wang et al*, 1995a; 1995b]. A full particle electrostatic PIC code is applied in this study. A typical simulation setup is shown in Fig. 3. The spacecraft is modeled as a 3 dimensional box structure with a conducting surface and a surface potential Φ_s relative to the ambient. An ion beam is injected to the low density ambient plasma in the x direction.

As discussed in the introduction, the problem studied here is different from a typical ion thruster problem where the beam flow is quasineutral. For comparison, we first present a typical simulation result for an ion thruster [*Wang et al*, 1996b]. Fig. 4 shows the potential contours and beam particle positions on a x-y plane cutting through the center of the thruster. In this case, the beam is quasi neutral and the spacecraft potential is much less that the kinetic energy of beam ions, $|\Phi_s| << \Phi_{bk0}$. Hence, the beam ions are not influenced by the potential field. The structure of the potential field is dominated by the disturbance from the high density ion beam. Since the electrons are much

more mobile than ions, the beam center has a higher potential.

We now simulate ion beam emissions with the neutralizer off. The simulation follows both the beam ions and the ambient electrons and ions. The simulation domain is initially loaded with ambient particles. The beam particles are injected into the simulation domain from the thruster exit at every time step.

We take the ambient plasma density $n_\infty \sim 5 \times 10^5$ and ambient plasma temperature $T_e = T_i \sim 1$eV. This is similar to a typical low Earth orbit environment. The ambient Debye length $\lambda_{D\infty} \sim 1$cm. We consider an ion beam with an initial kinetic energy $\Phi_{b0} = 1000$eV. We consider three beam current densities, as summarized in Table 1. The ambient ion current density is characterized by $J_{i\infty} = en_\infty C_s$, where $C_s = \sqrt{T_e/m_i}$. Hence the beam current densities considered are in the range of $J_{b0}/J_{i\infty} \sim 10^2 - 10^3$.

Since our emphasis is on the nearfield space charge effects, we set the simulation domain to be the downstream region of the beam emitting surface (including the thruster). The number of grid points used is $66 \times 33 \times 33$. The grid resolution is taken to be $d_{cell} = \lambda_{D\infty} \simeq 1$cm. The spacecraft surface is at $x = 0.5$. Other boundaries of the simulation domain represent the ambient where ambient electrons and ions are injected into the domain according to their thermal flux. The thruster body is located at $0.5 \le x \le 2.5$, $11 < y \le 23$, and $11 \le z \le 23$. The ion beam exit center is located at $x = 2.5$, $y = 17$, and $z = 17$, and the beam radius is $r_b = 6$. We consider a high spacecraft potential, $\Phi_s = -250$V, and a low spacecraft potential, $\Phi_s = 50$V.

The simulation variables are normalized as follow's: $\hat{t} = t\omega_{pe}$, $\hat{x} = x/\lambda_{D\infty}$, $\hat{v} = v/(d_{cell}\omega_{pe}) = v/v_{te}$, $\hat{\Phi} = \Phi/T_e$, and $\hat{n} = n/n_\infty$. An artificial ion to mass ratio $m_i/m_e = 100$ is used. Hence, the normalized initial beam velocity $\hat{v}_0 = \sqrt{(m_e/m_i)(\Phi_{ek}/T_e)} = 6$. The number of test particles used is in the range of 1.5×10^6.

In Fig.5 though Fig.10, we show simulation results on a xy plane cutting through the thruster center at $z = z_{thruster} = 22$ (the "center xy plane"). Results for case A1 ($\hat{J}_{b0} \simeq 63.3$) are shown in Figures 5 and 6. Unlike the situation shown in Fig.4, the potential structure in this case is clearly dominated by the sheath due to the surface potential. However, the sheath thickness is contracted within the beam region due to high beam density. The ambient electrons are repelled towards far right side by the negative surface potential. The ion beam space charge causes the beam to diverge near the right side of the simulation domain and draws ambient electron currents into the downstream beam region. As the v_x vs. x phase space plot shows, the beam velocity decreases monotonically. The potential alone the downstream axis of the thruster is plotted in Fig.11a, which shows a familiar monotonic profile for a sheath.

Results for case B1 ($\hat{J}_{b0} \simeq 316.2$) are shown in Figures 7 and 8. In this case, a positive potential hump develops near the beam exit ($\Phi_m \simeq 46$ at $x - x_{thruster} \simeq 13$). A population of electrons are trapped within that potential hump. The v_x vs. x phase space plot shows that the beam velocity decreases to a v_{xmin} at $x \simeq 15$ before accelerating towards right. The potential alone the downstream axis of the thruster is plotted in Fig.11b, which shows a nonmonotonic potential profile discussed in the last section. Since $\Phi_m << \Phi_{b0}$, the beam still flows mostly in the x direction. Due to larger beam density, the space charge effects is stronger than that in case A1 and causes a larger beam divergence. Although the 1-D theory qualitatively explains the potential hump, it is clearly no longer valid in this case. For a particle near the beam edge, it's dynamics is more similar to that of a particle undergoing orbit-limited motion near a probe in the thick-sheath regime. The beam divergence shielded the effect of the spacecraft potential and result in a much thinner sheath. As a result, electrons move into a region much closer to the spacecraft.

Results for case C1 ($\hat{J}_{b0} \simeq 3162.3$) are shown in Figures 9 and 10. In this case, a virtual anode has formed at $x - x_{thruster} \simeq 2$ The potential alone the downstream axis of the thruster which is plotted in Fig.11c, exhibits a potential $\Phi_m \sim \Phi_{b0}$. As the v_x vs. x phase space plot shows, some of the beam particles are accelerated back towards the beam exit. As evident from the $\hat{J}_b$ plot and ion position plot, the beam has lost its coherent structure. The ion current seems to originate from the virtual anode rather than flowing out from the thruster. On the other hand ambient electrons flows towards the virtual anode. The virtual anode essentially shielded out the potential of the spacecraft.

Since the flow is completely 3-dimension, the 1-D theory does not apply. However, it is still interesting to calculate the 1-D critical current density along the thruster downstream axis. We find the "inflection" point is at approximately $x \simeq 8$, and thus $x_{inf} \simeq 5.5$. Hence, the normalized 1-D critical current density for this case is

$$\hat{J}_{c-1D} = \frac{J_{c-1D}}{en_0 C_s} = \frac{4\sqrt{2}}{9}\frac{\hat{\Phi}_{b0}^{3/2}}{\hat{x}_{inf}^2} \simeq 428$$

Clearly, our emitting current density is $\hat{J}_0 >> \hat{J}_{c-1D}$. However, the real critical current for a 3-D situation is larger than $\hat{J}_{c-1D}$ because 3-D effects make it unfavorable for the virtual anode.

larger than $J_{c\text{-}1D}$ because 3-1) effects make it unfavorable for the virtual anode.

The results for the Φ_s =- - 50V cases are similar to that of the Φ_s = - 250V cases. Fig.1 1 also plots the potential profile along the thruster downstream axis for the Φ_s = - 50V. As evident from Fig. 11b, the effects of Φ_s is mainly cm the location of the potential hump (Lowering Φ_s moves the potential hump away from thruster exit). This is in agreement with the 1-D results of eq(14). However, the conditions for virtual anode formation is still controlled by the emitting current density.

4. Summary and Conclusions

We have developed a 3-1) particle simulation model to study ion beam emissions in space. Simulation results are presented for ion beam emissions into a low density space plasma under various emitting current densities and spacecraft potentials. The results show that a positive potential hump or a virtual anode may form near the exit point of the beam. Similar to the 1-D space charge flow in a diode, the follow characteristics sensitively depends on the beam energy and current density. However, for ion beam emissions in space, 3-D beam divergence due to space charge and interactions between the beam ambient plasma make the problem much more complex. We find that the properties of space charge flow is most sensitively controlled the interactions between the beam ions and the ambient plasma. The ambient conditions controls the location of the "inflection" point, thus the critical current density for virtual anode formation. The self-acljoslrrwllt in the plasma makes the conditions for virtual anode formation less favorable in ion beam emission in space. Nevertheless, unlike the situation of electron beam emissions where charge exchange ions can wipe out a nonmonotonic potential profile or a virtual cathode [*Intrator et al.*,1988], a nonmonotonic potential profile is a stable potential structure for ion beam emissions. Charge-exchange ions generated during ion thruster operation will enhence a positive potential hump near thruster exit,.

Acknowledgement

This work was carried out by the Jet Propulsion Laboratory, California Institute of Technology under a contract with NASA. Access to the Cray J90 supercomputer used in this study was provided by funding from NASA Offices of Mission to Planet Earth, Aeronautics, and Space Science.

References

[1] C.K. Birdsall and W.B. Bridges, Space-charge instabilities in electron diodes and plasma converters, *J. Appl. Phys.*, 32(17), p2611, 1961.

[2] C.D. Child, Discharge from hot CaO *Phys. Rev.*, 32, p492, 1911.

[3] Fay, C1., A.L. Samuel, and W. Shockley, On the Theory of Space Charge between Parallel Electrodes, *Bell Sys. Tech. J.*, 17(49), p49, 1938.

[4] T. Intrator, et al, The virtual cathode as a transient double sheath, *J. Apply. Phys.*, 64(6), p2927, 1988.

[5] S.T. Lai, A theoretical investigation of virtual electrode formation near the SCATHA satellite, *EOS.*, 60(46), 1979.

[6] S.T. Lai, An overview of electron and ion beam effects in charging and discharging of spacecraft, *IEEE Trans. Nucl. Sci.*, 36, p2027, 1989.

[7] P.R. Stannard et al, Analysis of the charging of the SCATHA (p78-2) satellite, *NASA CR-165348*,1981.

[8] J. Wang, P.C. Liewer, and V.K. Decyk, 3D electromagnetic plasma particle simulations on a MIMD parallel computer *Computer Physics Comm.*, 87, p35, 1995a.

[9] J. Wang, J'. Liewer, and E. Huang, 3-D particle-ill-cell with Monte Carlo collision simulations on three MIMD parallel computers, submitted to *J. Supercomputing*, 1995b.

[10] J. Wang and J. Brophy, 3-D Monte-Carlo particle-il]-cell simulations of ion thruster plasma interations, *AIAA 95-2826*,1995c.

[11] J. Wang, R. Biasca, and 1'. Liewer, , 3D electromagnetic Monte Carlo particle-in cell simulations of critical ionization velocity experiments in space *J. Geophys Res.*, 101(A1), p371, 1996a.

[12] J. Wang, J. Brophy, and D. Brinza 3 D simulations of NSTAR ion thruster plasma environments, *AIA A 96-3202,1* 996b.

Cases	Φ_{bk0}/T_e	n_{b0}/n_∞	$J_0/en_\infty C_s$	Φ_s/T_e	Φ_{b0}/T_e
A1	10^3	2	63.25	-250	750
A2				-50	950
B1	10^3	10	316.23	-250	750
B2				-50	950
C1	10^3	100	3162.3	-250	750
C2				-50	950

Table 1: Simulation cases

Figure Captions

Figure 1: Ion thruster (Upper). Space charge potential along the ion beam (Lower).

Figure 2: Illustration of 1-D nonmonotonic potential profile. a) beam flow between plane electrodes. b) beam emission to space.

Figure 3: Spacecraft model setup.

Figure 4: Quasineutral flow of ion beam emission from an ion thruster. a) potential profile. b) beam particle positions.

Figure 5: Space charge flow: Case A 1. a) potential profile. b) beam ion current density. c) ambient electron current density.

Figure 6: Space charge flow: Case A 1. a) ambient electron positions. b) beam ion positions. c) beam ion v_x vs. x phase space.

Figure 7: Space charge flow: Case 111. a) potential profile. b) beam ion current density. c.) ambient elect.rol) current density.

Figure 8: Space charge flow: Case 111. a) ambient electron positions. b) beam ion positions. c) beam ion v_x vs. x phase space.

Figure 9: Space charge flow: Case C1. a) potential profile. b) beam ion current density. c) ambient electron current density.

Figure 10: Space charge flow: Case C1. a) ambient electron positions. b) beam ion positions. c) beam ion v_x vs. x phase space.

Figure 11: Potential profile along thruster downstream axis. a) cases A 1 and A2. b) cases B1 and B2. c) cases C1 and C2.

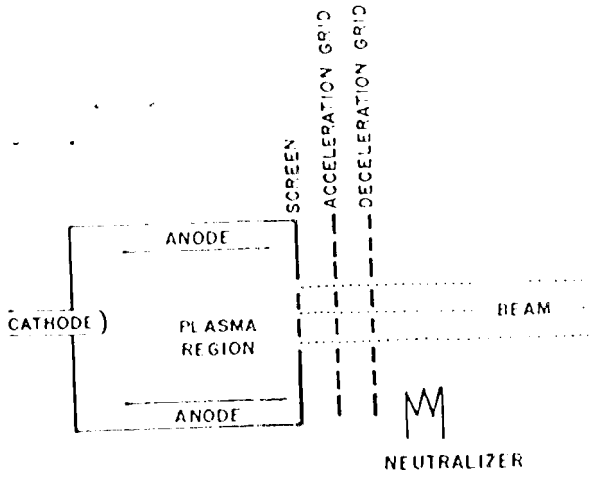

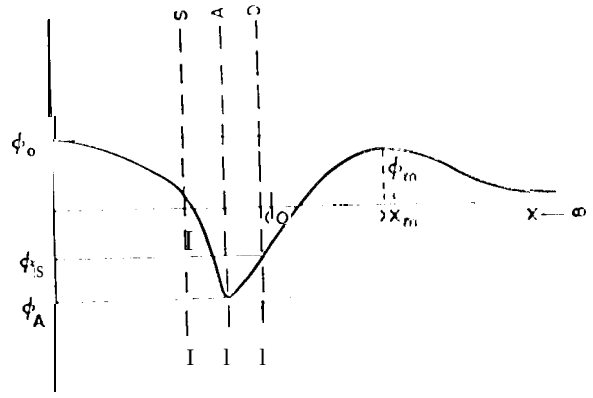

Figure 1

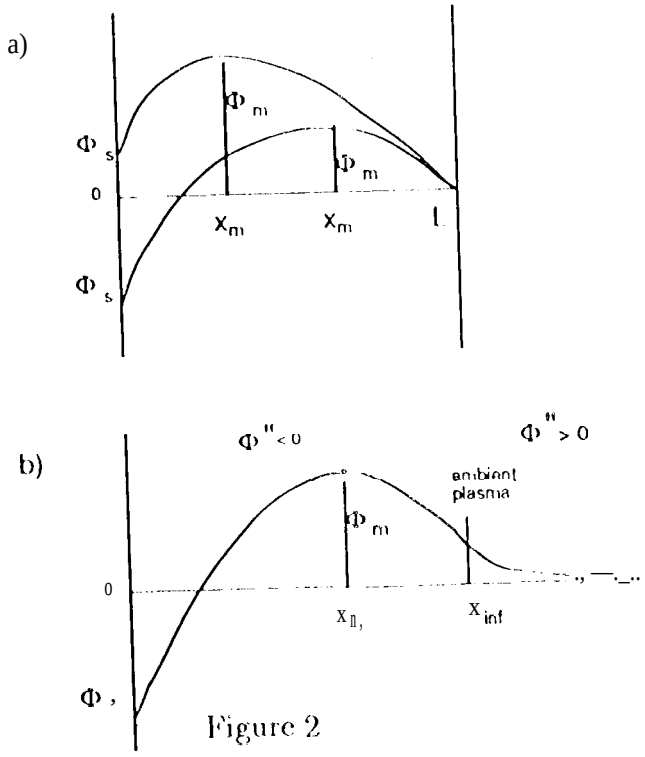

Figure 2

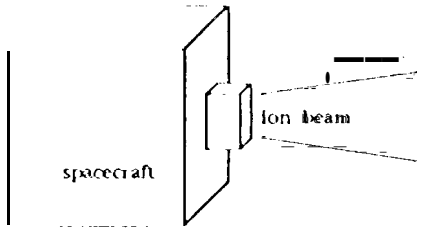

Figure 3

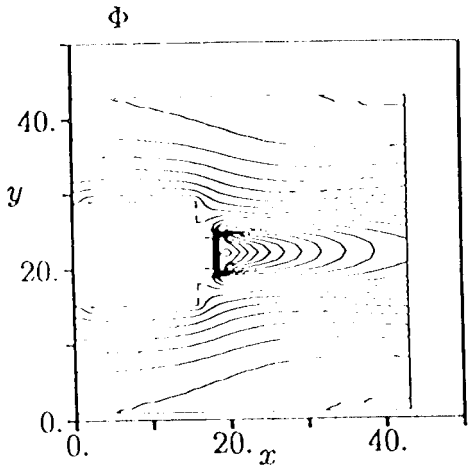

beam ion position

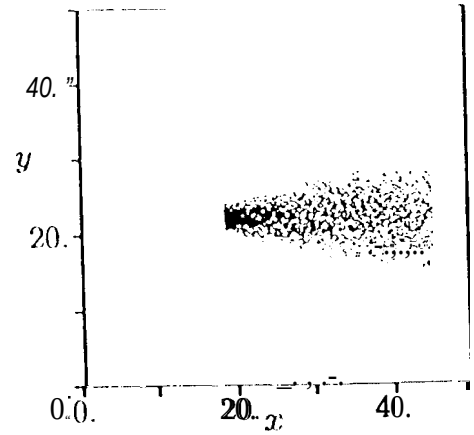

Figure 4

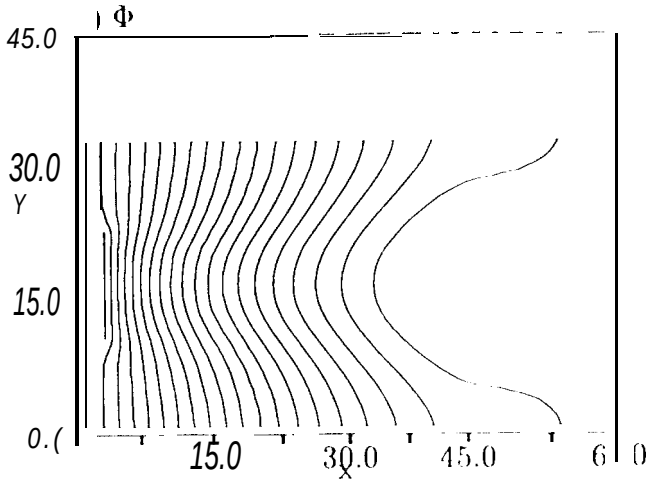

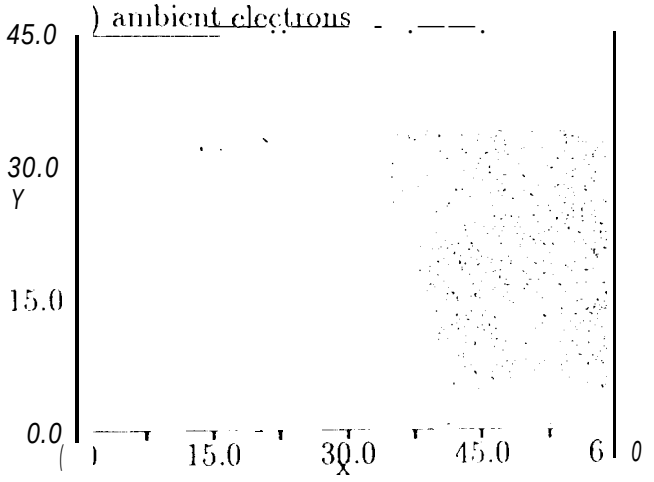

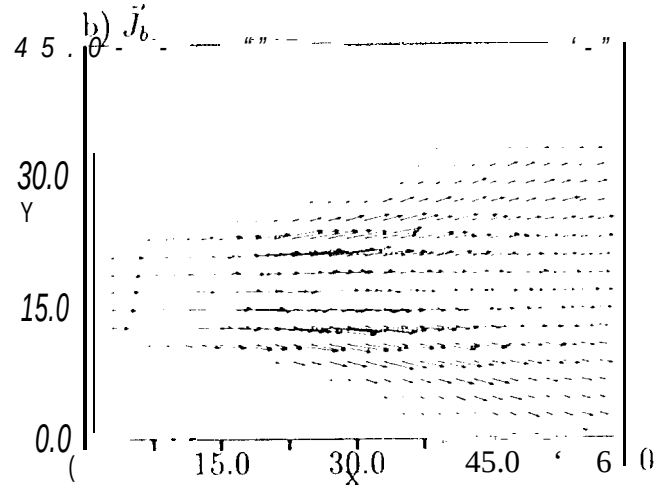

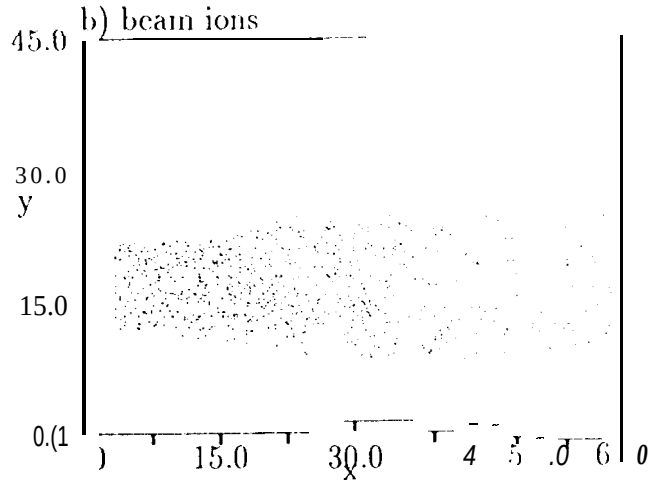

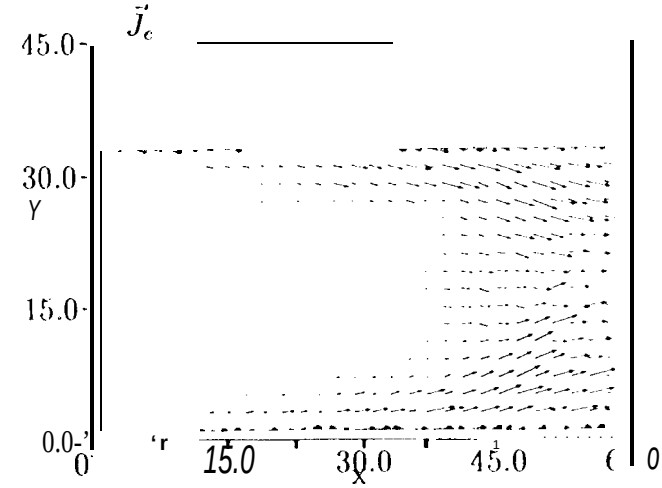

Figure 5

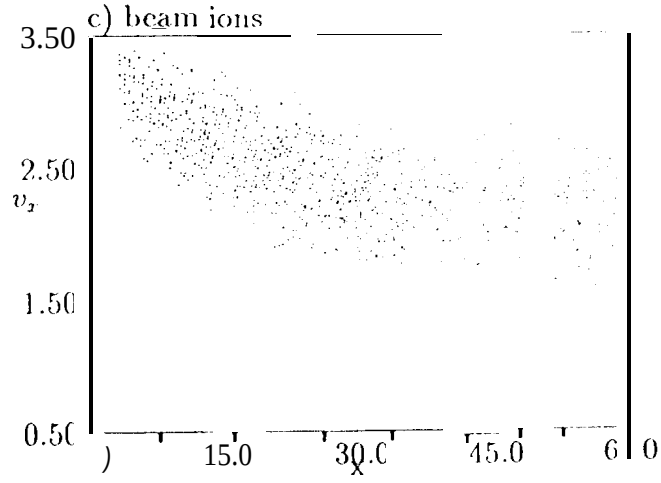

Figure 6

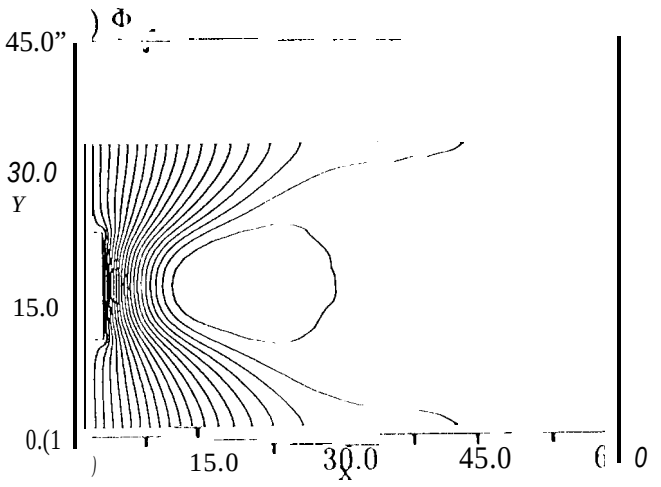

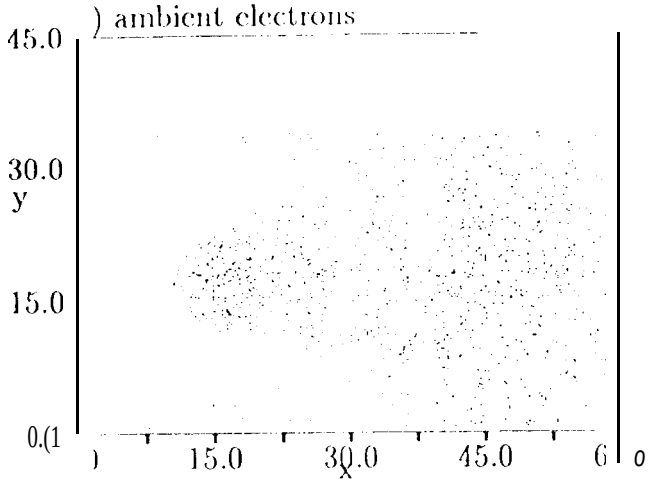

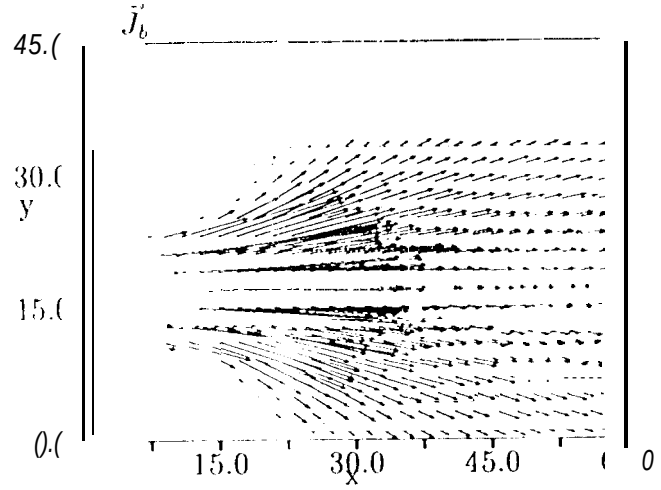

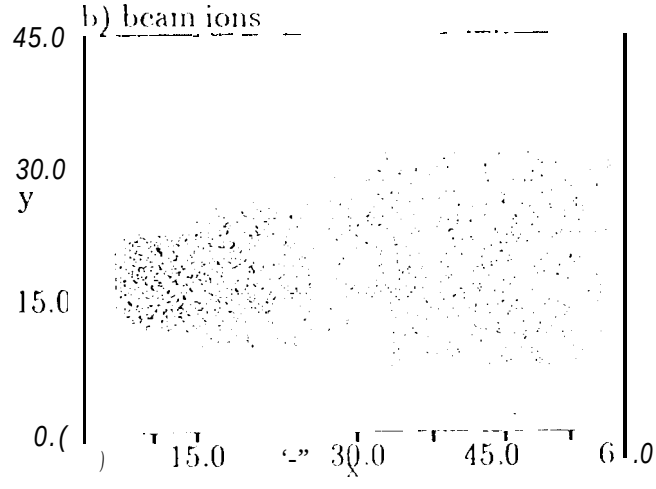

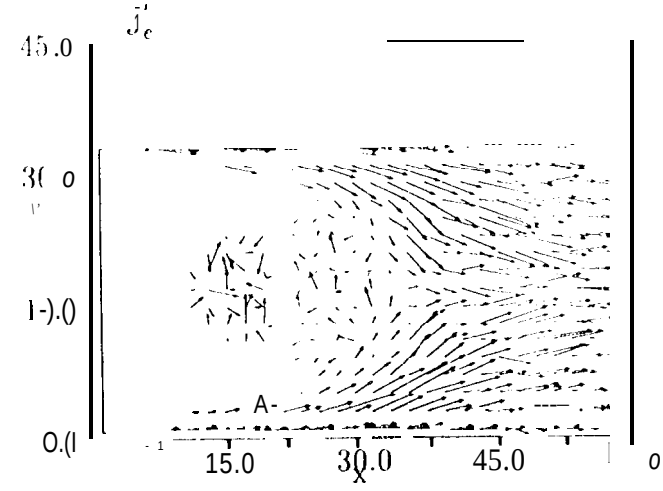

Figure 7

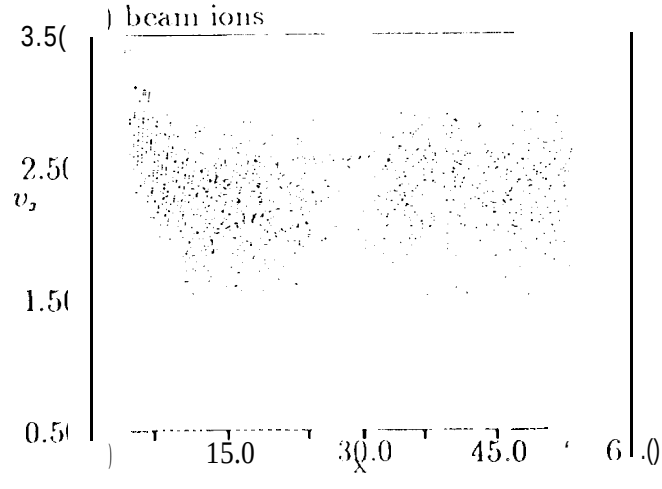

Figure 8

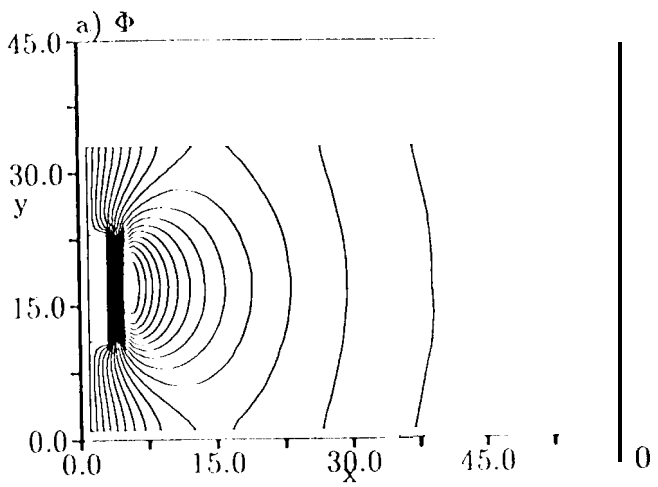

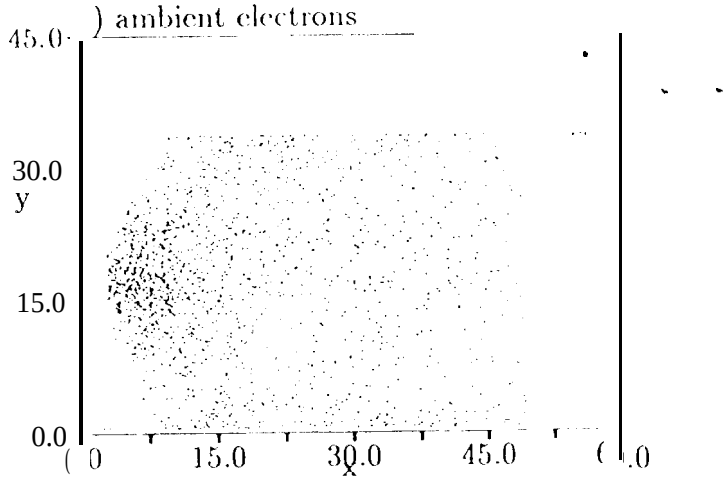

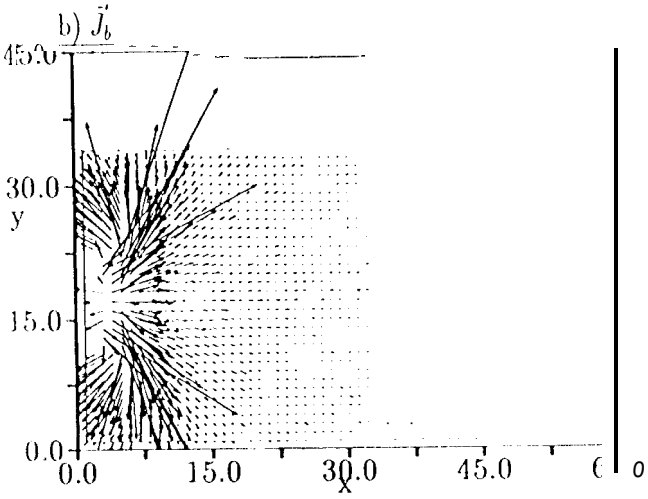

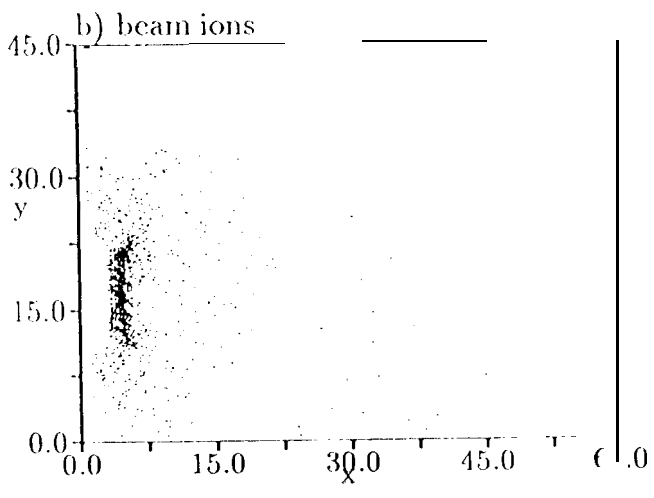

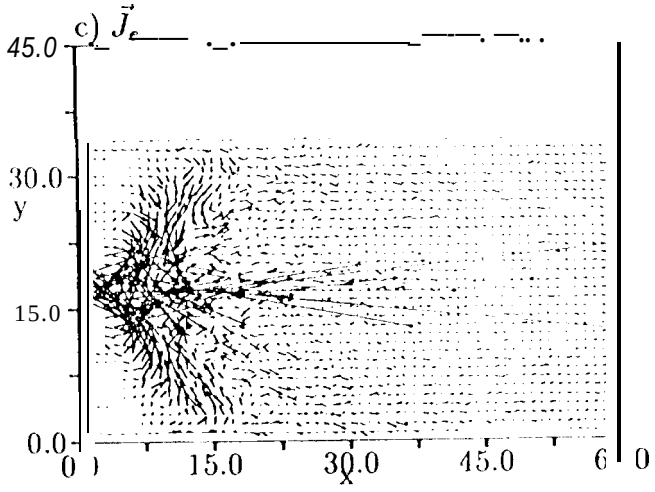

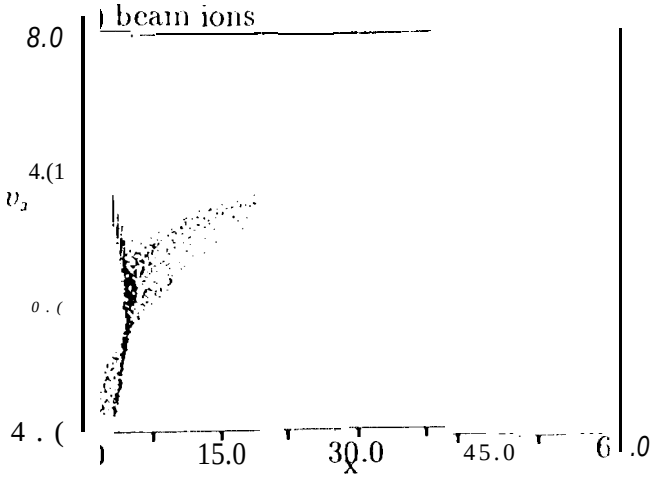

Figure 9

Figure 10

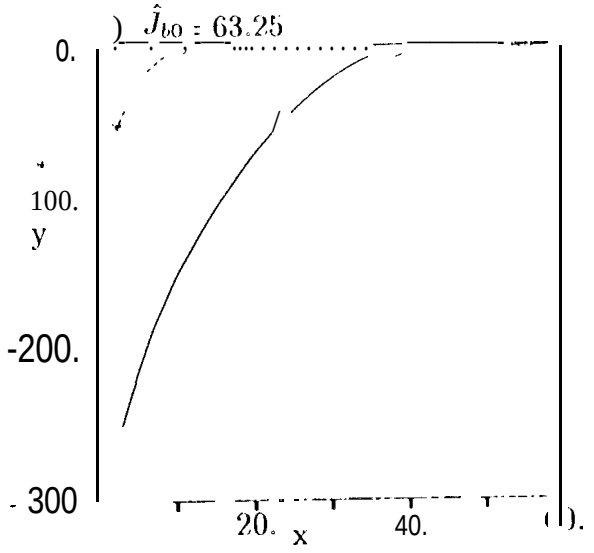
) $\hat{J}_{bo}$ = 63.25
0.
100.
y
-200.
- 300
20.
x
40.

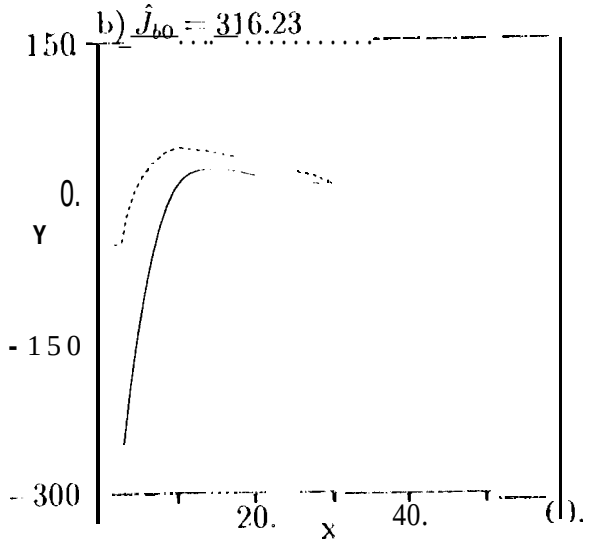
b) $\hat{J}_{bo}$ = 316.23
150
0.
Y
- 150
- 300
20.
x
40.

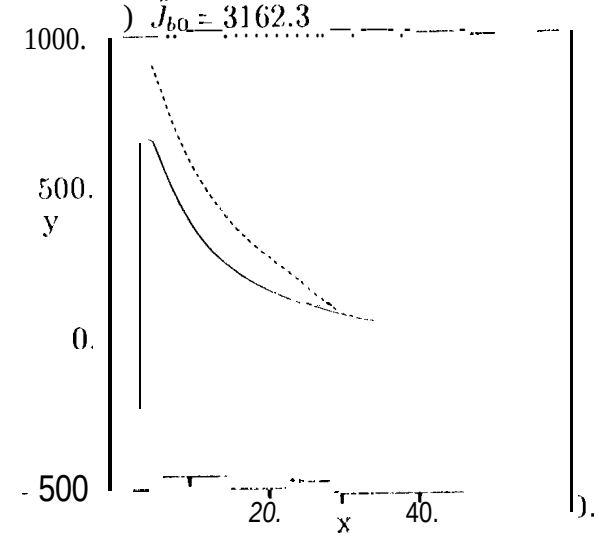
) $\hat{J}_{bo}$ = 3162.3
1000.
500.
y
0.
- 500
20.
x
40.

Figure 11